Small-angle X-ray scattering on the ChemMatCARS beamline at the Advanced Photon Source: a study of shear-induced crystallization in polypropylene

David Sutton,[a,b]* Tracey Hanley,[c,b] Robert Knott[a,b] and David Cookson[a,d]

[a]Bragg Institute, Australian Nuclear Science and Technology Organisation, Australia, [b]CRC for Polymers, Australia, [c]The School of Chemical Engineering and Industrial Chemistry, University of New South Wales, Australia, and [d]Australian Synchrotron Research Program, Australia.
E-mail: dsu@ansto.gov.au

The first ever time-resolved small-angle X-ray scattering (SAXS) data from the undulator 15-ID-D beamline (ChemMatCARS) are presented. A 1.3 Å (9.54 keV) X-ray beam was selected to study the structure development in a polypropylene sample during shear-induced crystallization. A Linkam CSS450 shear cell provided the temperature and shear control. The polypropylene was first melted and then quenched to the crystallization temperature, where a step shear was applied. The SAXS data were collected using a Bruker 6000 CCD detector, which provided images of excellent resolution. The SAXS images (with 180° rotational symmetry) indicated that the polypropylene crystallizes with a high degree of anisotropy, and the lamellae are oriented perpendicular to the flow direction.

Keywords: SAXS; ChemMatCARS; polypropylene; crystallization; shear.

1. Introduction

The application of time-resolved SAXS techniques for the study of polymer crystallization has developed into a powerful experimental tool, capable of providing a wealth of structural information to assist in the description of this complex process. If industrial polymer processing techniques, such as injection moulding, are to be understood and modelled effectively, then the mechanisms of shear-induced crystallization need to be investigated. This work forms part of a research program to investigate the properties of commercial grades of polypropylene, with a view to ultimately predicting the properties of injection moulded parts. The program has both a theoretical (Tanner, 2002) and an experimental approach, where the final morphology of injection moulded parts has already been studied using small- and wide-angle X-ray scattering (Liu *et al.*, 2002; Liu & Edward, 2001). Many other groups have investigated the crystallization characteristics of polypropylene (Heeley *et al.*, 2003; Koscher & Fulchiron, 2002; Göschel *et al.*, 2000; Gahleitner *et al.*, 2002; Somani, Yang & Hsiao, 2002). Current research studying model polypropylenes indicates that the long relaxation times of high-molar-mass polymer chains play an important role in the degree of orientation for samples crystallizing after a step shear (Seki *et al.*, 2002; Somani *et al.*, 2000; Haudin *et al.*, 2002; Heeley *et al.*, 2002). If industrial processing problems such as shrinkage and warpage are to be modelled and simulated accurately, then many factors will need to be considered in future studies, including the effect of molar mass and molar mass distribution, rubber toughening components and nucleating agents.

2. Experimental section

2.1. Beamline specification

The ChemMatCARS beamline receives X-rays from an undulator source, where the full monochromatic beam has an estimated flux of 10^{13} photons s^{-1} at 8 keV with an energy bandpass of 10^{-4}. The first optics enclosure (FOE) contains the beam-conditioning equipment and starts with a differential pump, which isolates the vacuum in the storage ring from the vacuum in the beamline. A collimator prevents the high-energy Bremsstrahlung γ-rays, created in the storage ring, from reaching the experimental hutch. Next, power-limiting apertures control the size of the X-ray beam and hence manage the power loading accepted by the monochromator. A Kohzu high-heat-load monochromator uses a water-cooled diamond (111) crystal to select the desired wavelength. A thermal dump then acts as a high-power beam stop to terminate the polychromatic wavelengths and protect the optics downstream. The first mirror has three coatings (Si, Rh, Pt) and acts as a low-pass filter to remove the high-order harmonics in the beam. A second mirror is used for further harmonic rejection and realignment of the beam. These two mirrors, deflecting in the vertical plane, provide a 1:1 focus to the sample. Next, an integral shutter controls whether or not the X-rays are allowed to pass onto the experimental hutch and can also act as a second thermal dump. The FOE ends with a specially polished and cooled X-ray transparent beryllium window. This window isolates the vacuum in the FOE from the vacuum in the shielded beam transport. The sample position has a 1 m floor footprint for the insertion of user-supplied equipment, in this case the shear cell, before the scattered X-rays pass through an evacuated flight tube onto the SAXS detector. Thus, with no horizontal focus (15 μrad divergence), a gentle vertical focus (<10 μrad) and an effective source size (H × V) of 250 μm × 20 μm, the 200 μm × 100 μm beam-defining slit allowed a total flux of about 10^{12} photons s^{-1} to the sample. As a result, the effective instrumental resolution was dominated by the point spread function of the Bruker 6000 charge-coupled device (CCD) detector (about 3 pixels or 500 μm full width at 10% maximum).

2.2. Polypropylene shear experiment

The polypropylene pellets (Basell Moplen EP301K) were first melt pressed to form bubble-free discs of approximately 700 μm thickness and about 15 mm in diameter. The polypropylene disc was loaded onto the Linkam CSS450 shear cell in a horizontal position. The quartz plates of the shear cell were replaced with stainless steel plates with windows of Kapton film (125 μm thick) to increase X-ray transmission. The shear cell was aligned such that the 200 μm × 100 μm (H × V) X-ray beam could pass through the centre of the 2.5 mm-diameter aperture, located at 7.5 mm from the centre of shear rotation. The polymer samples were melted at 483 K to erase any thermal/shear history. Once the polypropylene was molten, the upper plate was lowered to the desired sample thickness, in this case 500 μm. The shear cell was then placed in the X-ray beam path with the windows in a vertical position, such that the X-ray beam passed through the sample perpendicular to the shear direction. After 5 min at 483 K the sample was quenched to the crystallization temperature 403 K, at 30 K min^{-1}. A step shear was applied to the polypropylene at a shear rate of 50 s^{-1} for 10 s. The cessation of the applied shear was regarded as time zero for the SAXS data collection.

2.3. SAXS data collection

A Bruker 6000 CCD detector was used to collect the SAXS data. The detector has a data-collection area of 94 mm × 94 mm with a pixel size of 92 μm. The detector was located symmetrically at a

 doi:10.1107/S0909049504022873

distance of 1870 mm from the sample position, enabling a *d*-spacing in the range 40–1100 Å to be studied. A 2 mm-diameter beam stop protects the detector from the direct X-ray beam; no other beam attenuation was required. Data were collected for 6 s per frame followed by a 4 s wait period but, owing to a read-out time of about 3 s, the average time between frames was approximately 13 s. Exact frame times were captured from the file header information and used to create the time axis. The program *FIT2D* (Hammersley, 1997) was chosen to display the image files.

3. Results

The resulting SAXS images for the shear-induced crystallization of polypropylene are shown in Fig. 1. The colour scale of each image has been optimized to highlight small changes in the scattered X-ray intensity. The beam stop and its support arm are clearly visible casting a black shadow onto each image. The scattered X-rays remain isotropic until at least 13 s after the cessation of shear. By 26 s, large streaks appear in the meridional plane (flow direction) whilst there is also a small increase in scatter in the equatorial direction. The meridional streaks are oriented at about 5° to the horizontal plane, which is attributed to the curvature of the shear path seen within the aperture of the shear cell, implying that the smaller X-ray beam may not be located in the absolute centre of this aperture. The beam size also implies that a gradient of radii (and therefore shear rates) are being sampled, which must add to the complexity of the structures observed. The large increase in meridional scatter is attributed to the creation and orientation of semi-crystalline lamellae. These lamellae have become oriented perpendicular to the flow direction. The small increase in equatorial scatter was also observed in other samples in this study, and has been attributed, by Somani, Yang, Sics *et al.* (2002), to microfibrillar structures oriented parallel to the flow direction. These microfibrillar structures are often described as the shish in the shish kebab model. The image acquired at 39 s shows that there was a significant increase in scattering in all directions, whilst in the meridional plane the streaks have developed into lobes that exhibit 180° rotational symmetry. The next image at 51 s indicates that there has been an increase in the ordering of lamellae perpendicular to the flow direction, whilst a ring at the dominant scattering vector (**q**) can be seen most of the way around the image. The structure of the scattered intensity in the meridional peaks appears to coarsen from about 64 s onwards, the shape in the teardrop-like peaks remaining virtually unchanged. The long period in the meridional direction increases rapidly in the first 70 s to just under 300 Å. The size of the long period then decays slightly with time, as the structure perfects. The final coarsened SAXS image, collected at 2421 s after cessation of shear, indicates that a significant number of lamellar-like structures with a long period of about 265 Å become oriented perpendicular to the flow direction. However, a full ring at about this **q** value is present, indicating that similar structures have formed with all orientations. The step shear has induced nucleation and growth giving preferred lamellae orientation. The values obtained for the long period are typical for polypropylene, although precise values will depend on many factors such as molar mass, crystallization temperature and shear regime. Further studies confirm that the application of shear increases the crystallization kinetics with respect to crystallization under quiescent conditions.

4. Conclusions

The combination of extremely intense X-rays with very low divergence from a third-generation synchrotron, coupled with a high-resolution two-dimensional SAXS detector, produced a series of SAXS images of exceptional quality and detail. The only drawback with the existing set-up is the read-out time for the CCD detector which, at about 3 s, limits the study of faster processes even when the scattered count statistics may well be sufficient from a much shorter exposure time. The SAXS images following the shear-induced crystallization of polypropylene exhibit a high degree of anisotropy, with

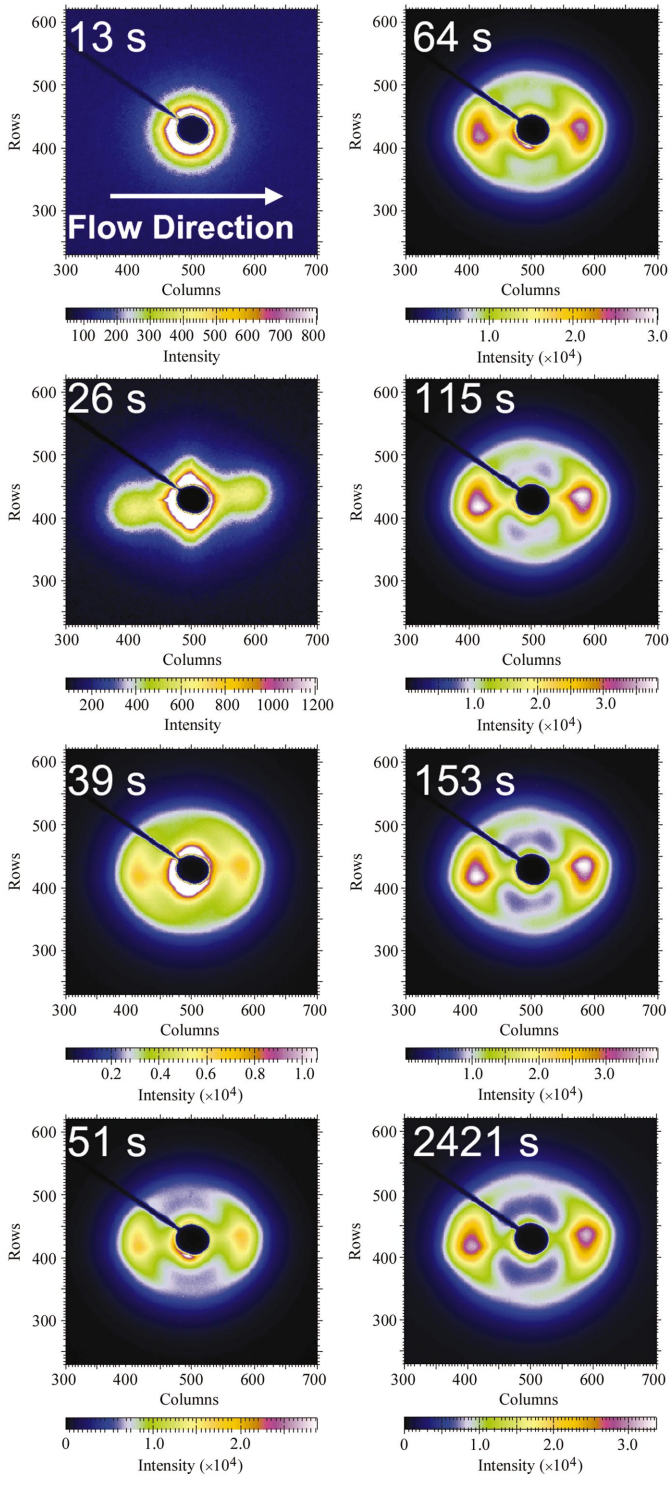

Figure 1
A selection of SAXS images for the shear-induced crystallization of polypropylene.

maxima in the meridional plane indicating lamellar-like structures oriented perpendicular to the flow direction. The images also exhibit 180° rotational symmetry.

Use of the ChemMatCARS Sector 15 at the Advanced Photon Source was supported by the Australian Synchrotron Research Program, which is funded by the Commonwealth of Australia under the Major National Research Facilities Program. ChemMatCARS Sector 15 is principally supported by the National Science Foundation/Department of Energy under grant number CHE0087817 and by the Illinois Board of Higher Education. The Advanced Photon Source is supported by the US Department of Energy, Basic Energy Sciences, Office of Science, under Contract No. W-31-109-Eng-38.

References

Gahleitner, M., Wolfschwenger, J., Fiebig, J. & Neißl, W. (2002). *Macromol. Symp.* **185**, 77–87.

Göschel, U., Swartjes, F. H. M., Peters, G. W. M. & Meijer, H. E. H. (2000). *Polymer*, **41**, 1541–1550.

Hammersley, A. P. (1997). ESRF Internal Report ESRF97HA02T. ESRF, Grenoble, France.

Haudin, J.-M., Duplay, C., Monasse, B. & Costa, J.-L. (2002). *Macromol. Symp.* **185**, 119–133.

Heeley, E. L., Maidens, A. V., Olmsted, P. D., Bras, W., Dolbnya, I. P., Fairclough, J. P. A., Terrill, N. J. & Ryan, A. J. (2003). *Macromolecules*, **36**, 3656–3665.

Heeley, E. L., Morgovan, A. C., Bras, W., Dolbnya, I. P., Gleeson, A. J. & Ryan, A. J. (2002). *Phys. Chem. Commun.* **5**, 158–160.

Koscher, E. & Fulchiron, R. (2002). *Polymer*, **43**, 6931–6942.

Liu, G. & Edward, G. (2001). *J. Inject. Mold. Tech.* **5**, 133–140.

Liu, G., Zhu, P. W. & Edward, G. (2002). *Macromol. Symp.* **185**, 327–340.

Seki, M., Thurman, D. W., Oberhauser, J. P. & Kornfield, J. A. (2002). *Macromolecules*, **35**, 2583–2594.

Somani, R. H., Hsiao, B. S., Nogales, A., Srinivas, S., Tsou, A. H., Sics, I., Balta-Calleja, F. J. & Ezquerra, T. A. (2000). *Macromolecules*, **33**, 9385–9394.

Somani, R. H., Yang, L. & Hsiao, B. S. (2002). *Physica A*, **304**, 145–157.

Somani, R. H., Yang, L., Sics, I., Hsiao, B. S., Pogodina, N. V., Winter, H. H., Agarwal, P., Fruitwala, H. & Tsou, A. (2002). *Macromol. Symp.* **185**, 105–117.

Tanner, R. I. (2002). *J. Non-Newton. Fluid Mech.* **102**, 397–408.

 Received 9 September 2003 • Accepted 14 September 2004